A Cuboid Geometry Design for MVDC Power Cables for Using in Future All Electric Wide Body Aircraft

Arian Azizi, Anoy Saha, and Mona Ghassemi
Zero Emission, Realization of Optimized Energy Systems (ZEROES) Laboratory
Department of Electrical and Computer Engineering, The University of Texas at Dallas, Richardson, TX, USA
arian.azizi@utdallas.edu, anoy.saha@utdallas.edu, mona.ghassemi@utdallas.edu

2023 IEEE Conference on Electrical Insulation and Dielectric Phenomena (CEIDP) | 979-8-3503-3562-0/23/$31.00 ©2023 IEEE | DOI: 10.1109/CEIDP51414.2023.10410513

Abstract- **Designing high-power-delivery and low-system-mass electric power systems (EPS) is a major goal to achieve the next generation of electrified aircraft. As one of its major components, cables must be redesigned to obtain high-power-density and low-system-mass EPS. Among challenges in designing aircraft cables such as arc and arc tracking, partial discharges (PD), and thermal management, the latter is decisive since the thermal properties of the cable determine its maximum ampacity. The maximum permissible current of a cable depends on radiative and convective heat transfers from its surface to the ambient environment. At the cruising altitude (12.2 km) of wide-body aircraft where the air pressure is 18.8 kPa, the convective heat transfer is greatly reduced which results in a reduction in maximum permissible current. Moreover, both radiative and convective heat transfers depend on the surface area of the cable. One way to increase the heat transfers and compensate for the reduction of convective heat transfer from a limited air pressure is to change the geometry of the cable. The cuboid geometry design provides a larger contact area with the ambient environment for the same cross-section area, so it is expected that the heat transfer will increase compared to conventional cylindrical cables, and in turn, the maximum power carrying capacity of the cable will be larger. Here, the question is whether the hypothesis is true, and if so, how much improvement can be expected. The purpose of this paper is to answer these questions and, for the first time, an MVDC (5 kVdc) high power (1 kA) cuboid shape cable is designed for future AEA to increase the maximum permissible current of the cable.**

I. Introduction

The transportation part accounts for the largest share (28%) of greenhouse gas (GHG) emissions in the United States in 2021. For upcoming generations of electrified aircraft, including all-electric aircraft (AEA) and more electric aircraft (MEA), their electric power systems (EPS) which is an islanded microgrid [1] will need to be able to deliver a high amount of power while maintaining a low overall system mass [2]. The cables which are responsible for the transmission and distribution of power across EPS show considerable potential for achieving mass savings due to their extended length. Electrical distribution and protection systems make up more than 30% of the total system mass. Implementing higher voltage operations is one strategy to reduce the mass of cables and, as a result, the total weight of the EPS of aircraft. In our previous research, three different ±5 kV bipolar MVDC EPS designs were presented for a potential wide-body AEA [3]. Arc and arc tracking, partial discharges (PD), and thermal management are among challenges in designing aircraft cables which are exacerbated by operating at 5 kV [4]. However, thermal management is decisive since it limits the maximum ampacity of the cables. At the cruising altitude of wide-body aircraft (12.2 km), the air pressure reduces to 18.8 kPa. This reduced air pressure significantly decreases the convective heat transfer compared to atmospheric pressure. It was shown that the maximum permissible current is reduced at the low pressure of cruising altitude of wide-body aircraft because of the reduced convective heat transfer [5-7]. Therefore, to further enhance the power density of the aircraft's EPS, cables must be redesigned to compensate for this reduction in the maximum permissible current at reduced air pressures. Heat loss in the core conductor of the cables is propagated to the ambient environment through radiative and convective heat transfers, which are affected by the surface area [7, 8]. The radiative heat transfer increases by increasing the surface area, however, the convective heat transfer may increase, decrease, or remain constant, since it is influenced by numerous factors which can disregard the growth in the surface area. Using cables in a cuboid shape is one way to increase the surface area while maintaining the same cross-sectional area and mass. As a result, the heat transfer through radiation and convection will change. Therefore, cuboid cables must be considered as a solution for compensating the reduction in the maximum permissible current at reduced pressures, while maintaining the same size and mass as the cylindrical cables. In this research, by using COMSOL Multiphysics, a finite element method (FEM) study is developed for analyzing a cable designed in a cuboid geometry and comparing its maximum permissible current to a conventional cylindrical cable. This model integrates electrical, thermal, and computational fluid dynamics (CFD) into a single study. The temperature and electric fields are also determined using this model for both cuboid and cylindrical cables. Calculating the temperature and electric fields simultaneously

II. Model

To evaluate the necessary characteristics of MVDC power cables operating at 18.8 kPa, an integrated electrical, thermal, and CFD model is required. A complex model has been previously developed in our prior study [5]. Southwire's 5 kV MVDC NL-EPR cable configuration is used in this study [9]. The characteristics of the cable are presented in Table I. The 2D

geometry of the cylindrical cable considered for modeling and simulations is depicted in Fig. 1. In typical uses, the cable may get up to 105℃ without being damaged [9]. This temperature is used to determine the cable's maximum permissible current.

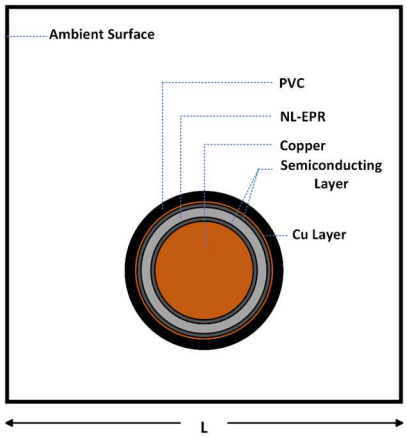

Fig. 1. The geometry of the cylindrical cable.

TABLE I: GEOMETRICAL CHARACTERISTICS OF THE CYLINDRICAL CABLE [9]

Parameters	Value
Conductor Diameter (mm)	28.372
Semiconductor Layer 1 Overall Diameter (mm)	29.769
NL-EPR Insulator Overall Diameter (mm)	34.341
Semiconductor Layer 2 Overall Diameter (mm)	35.865
Copper Layer Overall Diameter (mm)	36.119
PVC Jacket Overall Diameter (mm)	40.437
Maximum permissible temperature for normal condition (°C)	105

The cuboid shape cable considered for modeling and simulations is presented in Fig 2. Since the electric field is theoretically infinite at the sharp edges of a rectangle, we conducted our simulations using a geometry that has a cuboid shape with rounded corners. To have an equal cross-section area for both cuboid and cylindrical cables, one can show that:

$$L_C{}^2 = \pi\,(D/2)^2 K \tag{1}$$

$$r^2 = \left(L_C{}^2 - \pi\,(D/2)^2\right)/(4-\pi) \tag{2}$$

where, L_C is the length (m) of the cuboid cable, D is the diameter (m) of the cylindrical cable, r is the corner radius (m) of the rounded cuboid and K is the coefficient for the rounded corners. Since the surface area of the cylindrical and cuboid cables must remain the same, the coefficient K is utilized in this situation. With a K equal to 1, the cuboid cable shows completely sharp corners with 90 degrees, however, by increasing the K the corners of the cuboid cable tend to be more rounded, until at a certain K the cuboid cable shape completely changes to a cylindrical cable. In our research, we chose K to be 1.005 to have rounded corners without intensified electric field norm. The characteristics of the cuboid cable and the material properties of both cables are listed in Table II and Table III, respectively. Both cables' cross-sectional area and mass are the same. Also, all layers' thickness of the cuboid cable is the same as that of the cylindrical cable except the insulation thickness which is increased to have the same maximum electric field norm for both cables. However, effects of this increase on the total mass and size of the cuboid cable are negligible. The cables are placed in a duct filled with air. The air domain's boundaries are in contact with the duct's inner walls. The duct is a square shape made of aluminum.

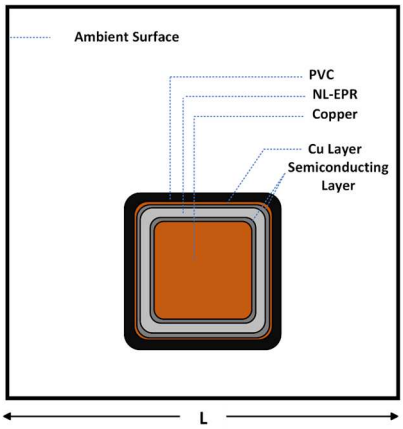

Fig. 2. The geometry of the cuboid cable.

TABLE II: GEOMETRICAL CHARACTERISTICS OF THE CUBOID CABLE

Parameters	Value
Conductor Length on one side (mm)	25.270
Semiconductor Layer 1 Overall Length (mm)	26.514
NL-EPR Insulator Overall Length (mm)	31.310
Semiconductor Layer 2 Overall Length (mm)	32.667
Copper Layer Overall Length (mm)	32.893
PVC Jacket Overall Length (mm)	36.015

TABLE III: THERMAL CHARACTERISTICS OF THE MATERIAL OF CABLES

Parameters	NL-EPR	PVC	Semiconductor
Thermal Conductivity (W.(m.K)$^{-1}$)	0.3	0.19	10
Heat Capacity (J.(Kg.K)$^{-1}$)	1800	1050	2405
Density (Kg.m^{-3})	860	1350	1055
Surface Emissivity	-	0.91	-

The thickness of the duct is 1 mm with a temperature equal to the ambient temperature and surface emissivity of 0.18. The cable is spaced 1 inch away from the floor side of the duct to ensure electrical safety. L, shown in Figs. 1 and 2, is the dimension of the duct's side and is assumed to be 250 or 1000 mm in this paper. The heat is conducted through the insulators, conductors, and PVC jackets. The heat equation from the conductor to the outer layer of the cable is given by:

$$\rho C_p \frac{\partial T}{\partial t} + \nabla.(-k\nabla T) = Q + q_o \tag{3}$$

where T is the temperature (K), ρ is the density (kg.m^{-3}), k is thermal conductivity (W.(K.m)$^{-1}$), C_P is the specific heat capacity at constant pressure (J.(kg.K)$^{-1}$), and q_o is the heat flux (W.m^{-3}). Net radiation exchange between the cable and the surrounding duct can be expressed as

$$q_{12} = \varepsilon_{eq}\sigma_S(T_S^4 - T_{amb}^4) \tag{4}$$

where T_s and T_{amb} are respectively temperature (K) of the surface of the cable and the ambient temperature, σ_S is Stefan's constant (W/(m^{2}K^4), and ε_{eq} is equal emissivity as

$$\varepsilon_{eq} = \frac{A_1}{\frac{1-\varepsilon_1}{\varepsilon_1} + \frac{1}{F_{12}} + \frac{1-\varepsilon_2}{\varepsilon_2\left(\frac{A_2}{A_1}\right)}} \tag{5}$$

where A_1 and A_2 are the area of the cable surface and ambient surface, respectively, ε_1 and ε_2 are their surface emissivity, and F_{12} is the view factor represented as

$$F_{12} = \frac{1}{A_1}\int_{A_1}\int_{A_2} \frac{cos\theta_1 cos\theta_2}{\pi R^2} dA_1 dA_2 \quad (6)$$

where R is the linking line between the surfaces, dA_1 and dA_2 are elemental areas, θ_1 and θ_2 are polar angles created by R and surface normal. Also, natural heat convection is responsible for transferring heat in the air domain. Details about natural heat convection can be found in [5]. The DC conductivity of polymers can be expressed by empirical formulas such as:

$$\sigma(E,T) = Aexp\left(\frac{-\varphi q_e}{k_b T}\right)\frac{\sinh(B(T)\ln(E))}{E^{\gamma}} \quad (7)$$

where q_e is the electron charge, k_b is Boltzmann's constant, E is the electric field (V.m^{-1}), φ is the thermal activation energy, σ_0, A and γ are constants, and $B(T)$ is a parameter that depends on the temperature. Details about Eq. (7) can be found in [5]. The electric field distribution is calculated by

$$E = -\nabla V \quad (8)$$

$$J_e = \sigma E \quad (9)$$

where J_e is the current density (A.m^{-2}), V is the voltage (V), and σ is the conductivity (S.m^{-1}). The temperature, velocity, and electric fields are coupled, as shown by Eqs. (3)–(9). For details, see [5-8]. To reach the steady case, the study time is determined to be 30 hours.

III. Results

Figs. 3 and 4 show the maximum permissible current of the cuboid and cylindrical cables at the pressure of 18.8 kPa when the duct's temperature changes between 20°C to 65°C for duct sizes of 250 mm and 1000 mm, respectively. The maximum permissible current of the cuboid cable is higher at all ambient temperatures compared to the cylindrical cable for both duct sizes. While the difference between the maximum permissible current of both cables remains approximately constant, the maximum permissible current decreases for both cables when the ambient temperature increases, resulting in higher growth in the maximum permissible current of the cuboid cable compared to the cylindrical one for higher ambient temperatures. The maximum difference between the maximum permissible current of the cables occurs at 65°C, 3% and 4.6% higher for duct sizes of 250 mm and 1000 mm, respectively. The results show that the growth in the maximum permissible current is larger for the duct size of 1000 mm, mainly because for the 1000 mm duct, radiative heat transfer constitutes a larger share of total heat transfer compared to the 250 mm duct as shown in Figs. 5 and 6. The growth in the maximum permissible current of the cuboid cable compared to the cylindrical one can be explained by increased radiative and convective heat transfers as shown in Figs. 5 to 8. The radiative heat transfer depends on the surface area of the cable, therefore, by increasing the surface area of the cable, the radiative heat transfer increases. The outer surface area of the cuboid cable is larger than the cylindrical cable, yielding a larger radiative heat transfer. However, according to Eq. (5), for the duct size of 1000 mm, the ε_{eq} is less sensitive to the surface emissivity of the duct compared to the duct size of 250 mm, meaning that the surface area of the cables affects the radiative heat transfer more linearly.

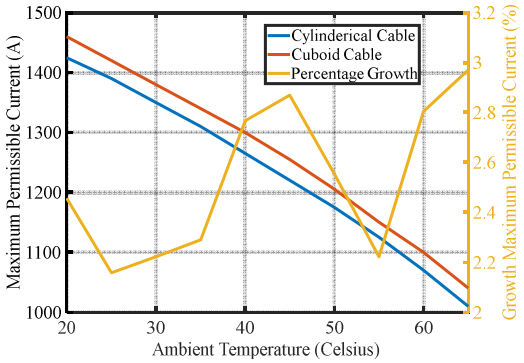

Fig. 3. Maximum permissible current of the cuboid and cylindrical cables at the pressure of 18.8 kPa for duct size of 250 mm

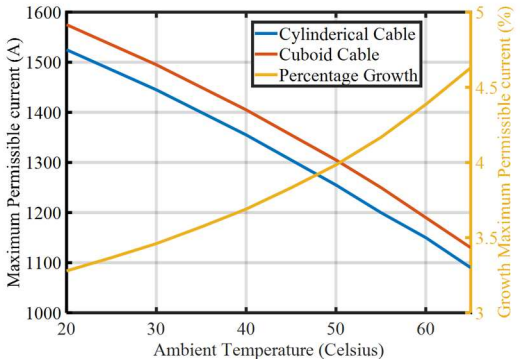

Fig. 4. Maximum permissible current of the cuboid and cylindrical cables at the pressure of 18.8 kPa for a duct size of 1000 mm

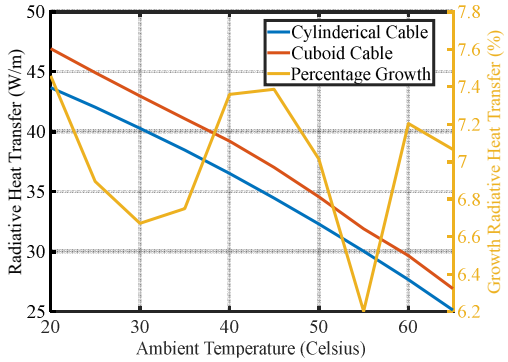

Fig. 5. Radiative heat transfer for the cuboid and cylindrical cables at the pressure of 18.8 kPa for a duct size of 250 mm

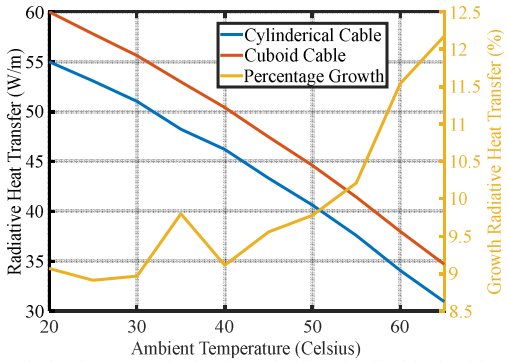

Fig. 6. Radiative heat transfer for the cuboid and cylindrical cables at the pressure of 18.8 kPa for a duct size of 1000 mm.

While the radiative heat transfer is different for the cuboid and cylindrical cables, the convective heat transfer is the same as shown in Figs. 7 and 8, showing that the increase in the surface area is somehow canceled out by other factors influencing the convective heat transfer, such as the velocity field in the vicinity of the cable and the share of the cable that is affected by that velocity field. The growth in the convective heat transfer for the duct size of 1000 mm is larger than that of 250 mm, primarily due to the smaller amount of convective heat transfer. Fig. 9 shows the electric field across the cuboid and cylindrical cables. The maximum electric field is the same for both cables since the thickness of the insulation of the cuboid cable is designed to be larger than the cylindrical one. Also, the electric field inversion, which means a larger electric field norm at outer radii or distances from the conductor, occurs for both cables. Moreover, the electric field norm at the rounded corners of the cuboid cable is not intensified, as it is designed to be. In our other studies, a coaxial geometry design was studied in [10, 11] while the influence of vertical and horizontal arrangements of a conventional bipolar cable on the maximum permissible current of the cable was studied in [12].

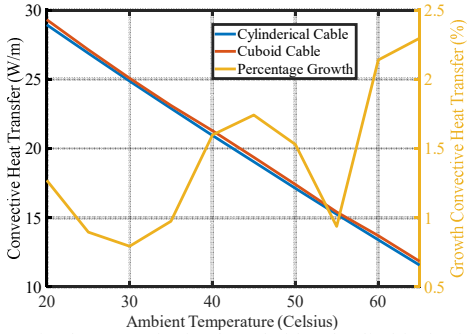

Fig. 7. Convective heat transfer for the cuboid and cylindrical cables at the pressure of 18.8 kPa for a duct size of 250 mm.

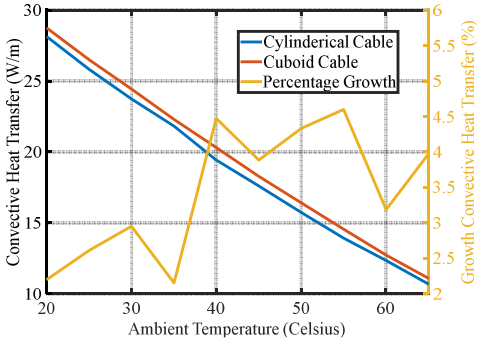

Fig. 8. Convective heat transfer for the cuboid and cylindrical cables at the pressure of 18.8 kPa for a duct size of 1000 mm.

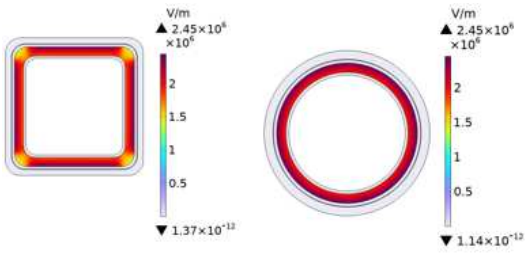

Fig. 9. Electric field distribution across the cuboid and cylindrical cables when the conductor's temperature is 105°C.

IV. Conclusion

In this paper, for the first time, a cuboid MVDC cable for future AEA is designed and analyzed by developing a coupled electrical, thermal, and computational fluid dynamics model in COMSOL software. The aim is to increase the maximum permissible current while maintaining the same size and mass as conventional cylindrical cables. For the cuboid cable, the maximum permissible current increases by 3% and 4.6% in comparison to the conventional cylindrical cable for duct sizes of 250 mm and 1000 mm. Also, it was shown that this increase in maximum permissible current is resulted from the increased radiative and convective heat transfers for the cuboid cable. However, these growths are different for the duct sizes of 250 and 1000 mm, larger for the latter.

Acknowledgment

This work was supported in part by the U.S. Advanced Research Projects Agency-Energy (ARPA-E) under Award DE-AR0001677, in part by the U.S. National Science Foundation (NSF) under Award 2306093, and in part by the U.S. Air Force Office of Scientific Research under Award FA9550-20-1-033.

References

[1] M. Hamidieh and M. Ghassemi, "Microgrids and resilience: A review, " *IEEE Access*, vol. 10, pp. 106059–106080, Oct. 2022.

[2] A. Barzkar and M. Ghassemi, "Components of electrical power systems in more and all-electric aircraft: A review," *IEEE Trans. on Transp. Electrific.*, vol. 8, no. 4, pp. 4037–4053, Dec. 2022.

[3] M. Ghassemi, A. Barzkar, and M. Saghafi, "All-electric NASA N3-X aircraft electric power systems," *IEEE Trans. Transp. Electrific.*, vol. 8, no. 4, pp. 4091–4104, 2022.

[4] G. J. Anders, *Rating of Electric Power Cables in Unfavorable Thermal Environment*. Hoboken, NJ: Wiley, 2005.

[5] A. Azizi, M. Ghassemi, and J. M. Lehr, "Heat transfer challenges for MVDC power cables used in wide body all electric aircraft under low pressures," *IEEE Access*, vol. 10, pp. 111811–111819, 2022.

[6] A. Azizi, M. Ghassemi, and J. Lehr, "Influence of low pressure on thermal limit of MVDC power cables used in all electric aircraft," *IEEE Int. Power Modulator and High Voltage Conf. (IPMHVC)*, 2022, pp. 88–91.

[7] A. Azizi and M. Ghassemi, "Design of high power density MVDC cables for wide body all electric aircraft," *IEEE Trans. Dielectr. Electr. Insul.*, Early Access, 2023, doi: 10.1109/TDEI.2023.3285849.

[8] A. Azizi, M. Ghassemi, and J. Lehr, "Design of a cable system for a high-power density MVDC aircraft electric power system," *IEEE Conf. Elect. Insul. Dielectr. Phenomena (CEIDP)*, 2022, pp. 151–154.

[9] "1/c CU 5kv 90 NLEPR 100% PVC MV-105," Southwire, https://www.southwire.com/wire-cable/medium-voltage-power-cable/1-c-cu-5kv-90-nlepr-100-pvc-mv-105/p/MV20 (accessed May 30, 2023).

[10] A. Saha, A. Azizi, and M. Ghassemi, "An optimal bipolar MVDC coaxial power cable design for envisaged all electric wide body aircraft," *IEEE Conf. Electrical Insul. Dielectric Phenomena (CEIDP)*, 2023.

[11] A. Saha, A. Azizi, and M. Ghassemi, "Optimal bipolar MVDC power cable designs for future wide-body all electric aircraft," *IEEE Trans. Dielectr. Electr. Insul.*, submitted for publication.

[12] A. Azizi and M. Ghassemi, "A FEM coupled electrical, thermal, and computational fluid dynamic model and a theoretical Model for calculation of maximum permissible current in envisaged wide-body all-electric aircraft bipolar MVDC power cables," *IEEE Trans. Dielectr. Electr. Insul.*, submitted for publication.